Compatibility of Lead-Free Solders with Lead Containing Surface Finishes as a Reliability Issue in Electronic Assemblies

Paul Vianco and Jerry Rejent
Sandia National Laboratories
Albuquerque, NM

Iris Artaki, Urmi Ray, Donald Finley, and Anna Jackson
AT&T Bell Laboratories, Engineering Research Center
Princeton, NJ

Abstract

Enhanced performance goals and environmental restrictions have heightened the consideration for use of alternative solders as replacements for the traditional tin-lead (Sn-Pb) eutectic and near-eutectic alloys. However, the implementation of non-Pb bearing surface finishes may lag behind solder alloy development. A study was performed which examined the effect(s) of Pb contamination on the performance of Sn-Ag-Bi and Sn-Ag-Cu-Sb lead-free solders by the controlled addition of 63Sn-37Pb solder at levels of 0.5 - 8.0 wt.%. Thermal analysis and ring-in-plug shear strength studies were conducted on bulk solder properties. Circuit board prototype studies centered on the performance of 20I/O SOIC gull wing joints. Both alloys exhibited declines in their melting temperatures with greater Sn-Pb additions. The ring-in-plug shear strength of the Sn-Ag-Cu-Sb solder increased slightly with Sn-Pb levels while the Sn-Ag-Bi alloy experienced a strength loss. The mechanical behavior of the SOIC Sn-Ag-Bi solder joints reproduced the strength drop to Sn-Pb contamination; however, the strength levels were insensitive to 10,106 thermal cycles. The Sn-Ag-Cu-Sb solder showed a slight decrease in the gull wing joint strengths that was sensitive to the Pb content of the surface finish.

1. Introduction.

The electronics industry continues to be shaped by advances in the technologies of chip architecture, packaging, and substrate materials. Increased chip functionality has demanded higher I/O counts on the packages. The result has been I/O alternatives to the traditional peripherally leaded packages, in particular, the area array configuration (e.g., Pin Grid Array, Ball Grid Array, and chip scale packages). As larger package sizes (and smaller solder joints) are introduced into surface mount applications, the choice of substrate and package materials has become increasingly critical towards achieving acceptable product reliability, particularly under thermal cycling environments.

In addition to these technological "drivers," the electronics industry is also examining the environmental compatibility of its manufacturing processes. For example, alternative cleaning processes were implentented when the Montreal Protocol Agreements restricted, and in some cases banned, the use of chlorofluorocarbon (CFC) solvents[1]. Similar concerns are being raised about the use of Pb-bearing solders in electronic products, in particular, the potential for ground water contamination from discarded electronic assemblies.

Advancing technology and an increased concern for the environment has caused circuit board designers and manufacturers to consider the use of alternative solders for the assembly of electronic products. In recent years, a number of studies have been conducted that examined alternative, Pb-free solders for circuit board assembly[2-5]. These studies have included the development of several new solder compositions[6-8]. The newer alloys, as well as long-standing commercial solders (developed primarily to meet the ban on lead-bearing solders for potable water systems), have been assessed for manufacturability and reliability on prototype test vehicles. Both surface mount and through-hole technologies have been evaluated in the cited works.

In the course of those prototype studies, it was deemed prudent to restrict the surface finishes of the circuit boards and package I/O's (leads or terminations) to non-lead bearing coatings. Immersion tin, organic solderability preservatives, and precious metal coatings were used in those experiments. This approach was taken for two reasons. First of all, it was construed that removal of the Pb hazard must necessarily include the elimination of Pb-bearing solder coatings on I/O's and circuit board features. Secondly, the metallurgy of the Pb-free solders necessitated that Pb be eliminated from the joint due to the potential formation of low melting temperature phases within the newer solder compositions. These phases could not only jeopardize the room temperature mechanical integrity of the solder, but also limit the upper service temperature of the alloy.

Although it was feasible to obtain test vehicles with the desired, non-Pb finishes in small (experimental) quantities, further inquiry quickly revealed that the electronics industry infrastructure comprised of component manufacturers and circuit board producers would not readily convert to the alternative finishes. Therefore, it was decided that a more in-depth analysis of the effects of Pb contamination on the performance of alternative solders should be conducted.

The first of the two solders selected for this study was a commercially available alloy, 96.2Sn-2.5Ag-0.8Cu-0.5Sb (wt.%) designated by the tradename, CASTIN™ (A.I.M. Corp.). This solder had an "onset" temperature of 218.7°C (as determined by Differential Scanning Calorimetry, or DSC, at a heating rate of 10°C/min). The onset temperature appeared to represent a eutectic phase transformation since individual solidus and liquidus peaks could not be distinguished from the single peak on the output thermogram. An optical micrograph of the solder microstructure appears in Fig. 1a. The Sn matrix

of the solder contained a network of Ag_3Sn particles resulting from the dendritic growth of this latter phase. The limited Sb and Cu remained largely in solid solution in the Sn-matrix.

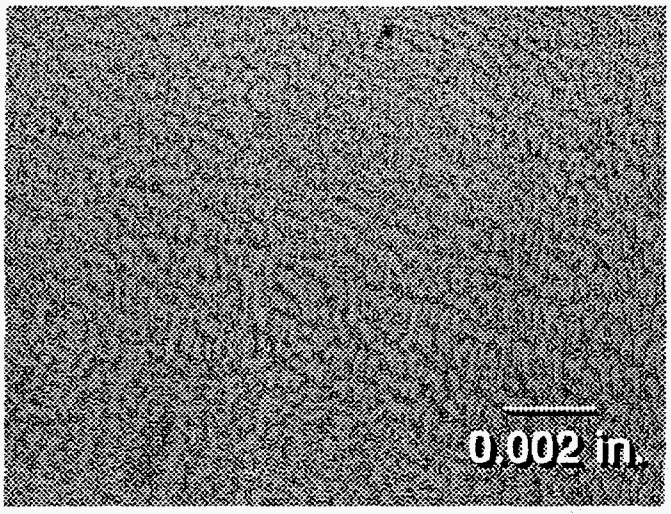

(a)

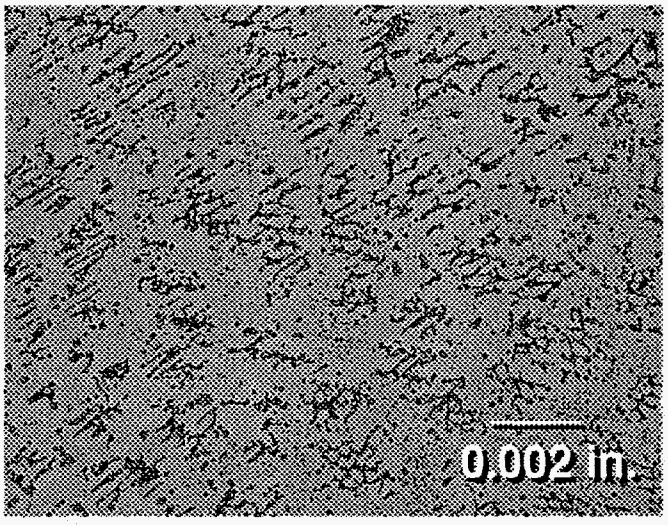

(b)

Fig. 1 Optical micrographs of the solder alloys (a) CASTIN™ and (b) 91.83Sn-3.33Ag-4.83Bi (wt.%). All samples were cooled at 10°C/min.

The second solder was an experimental composition, 91.83Sn-3.33Ag-4.83Bi[9]. This alloy had an onset temperature of 212°C. As with the CASTIN™ alloy, the solidus and liquidus peaks of the Sn-Ag-Bi solder could not be separated from the singly observed peak, even at a reduced heating rate of 1°C/min. An optical photograph of the solder microstructure appears in Fig. 1b; it is comprised of a Sn matrix and isolated colonies of Ag_3Sn particles. The Bi is largely in solid solution in the Sn matrix.

The selection of both solders for this study was based upon previous performance marks[2,6]. The two solders had demonstrated very good wetting properties in both laboratory tests as well as on prototype circuit boards. Early thermal fatigue tests on the Sn-Ag-Bi solder prototypes demonstrated excellent stability against fatigue damage[5].

In the first part of the study described in this report, (a) melting point, (b) wettability, and (c) ring-in-plug shear strength properties were evaluated for CASTIN™ and Sn-Ag-Bi solders which had been contaminated with controlled quantities of Pb. The Pb was added in the form of 63Sn-37Pb solder; the appropriate quantities of Sn-Pb additions represented an *upper* range of contamination levels that could be expected from typical through-hole and surface mount solder joints.

The second segment of this study used the CASTIN™ and Sn-Ag-Bi solders on prototype mixed technology circuit boards. Only the surface mount test vehicle results will be presented. The assessment of solder joint performance centered upon the pull strength of 50 mil pitch, 20 I/O Small Outline Integrated Circuit (SOIC) package, gull wing leaded solder joints. Tests were performed on the as-fabricated joints as well as joints that were exposed to thermal cycle accelerated testing.

2. Experimental.

2.1. Bulk alloy properties measurements.

2.1.1. Fabrication of Pb-contaminated solder alloys.

The addition of Pb to the CASTIN™ and Sn-Ag-Bi solders was performed by combining 63Sn-37Pb (Sn-Pb) alloy into each of the two test solders. This methodology permitted the addition of relatively small absolute quantities of Pb, without the need to make large batches of material in order to minimize concentration errors. Also, the Pb dissolved more quickly into the solder batches as the Sn-Pb solder composition rather than pure Pb because of the former material's lower melting temperature and relatively limited oxide thickness.

The Sn-Pb additions were based upon computations of the potential Sn-Pb contamination from (1) a typical plated through-hole solder joint and (2) a 1206 leadless chip capacitor solder joint. First, the through-hole case is described. It was assumed that the joint was comprised of a 0.032 in. diameter lead and a 0.050 in diameter hole; the Sn-Pb solder coating thickness of these two structures were 0.0002 in. and 0.002 in., respectively. The pad was assumed to be an annular ring of 0.080 in. outer diameter. The meniscus rise was assumed to be 0.080 in. and of a triangular profile to facilitate calculation of the CASTIN™ and Sn-Ag-Bi solder volumes. The computed Sn-Pb solder contamination for this joint configuration was approximately 1.5 wt.%. This value translates into an actual Pb contamination of 0.9 wt.%.

Contamination of the 1206 chip capacitor solder joint was based upon a 63Sn-37Pb coating of 0.002 in. on both the circuit board pad and the chip termination. The amount of CASTIN™ and Sn-Ag-Bi solder in the joint was determined by the screen printer stencil thicknesses of 0.006 and 0.010 in. The resulting Sn-Pb contamination levels were between 3 wt.% and 5 wt.%. The corresponding Pb levels were from 2 wt.% to 3 wt.%. These values exceeded those of the typical through-hole joint because of the relatively small amount of solder contained in surface mount joints.

The results of the through-hole and surface mount contamination levels were combined to define a Sn-Pb contamination range of the discrete levels: 0.5, 1, 2, 4, 6, and 8%. The lower values would pertain to the through-hole case and the higher levels to the surface mount joints.

Each of the contaminated CASTIN™ and Sn-Ag-Bi solders were manufactured in approximately 0.5 lb lots from which samples were used for properties measurements.

2.1.2. Thermal (melting) properties measurement.
The melting properties of the bulk alloys were determined by Differential Scanning Calorimetry (DSC). The solder samples were placed into aluminum pans and tested under flowing nitrogen. The test temperature limits were 25°C and 300°C. Each sample was initially heated to 300°C at 20°C/min and subsequently cooled back to room temperature. A second run from which the actual test data were taken, was performed at 10°C/min. The "onset" temperature of a sited peak was determined from the projected temperature value for the intersection of the baseline and a line drawn through the inflection point on the peak's leading edge, parallel to the trace of the peak (i.e., the so-called "onset" technique).

2.1.3. Wettability test measurements.
The wettability of the contaminated solders was determined by the meniscometer/wetting balance technique. The details of the experimental procedure can be found in Reference[10]. Briefly, this technique quantifies the wetting performance through the contact angle, θ_c, formed by a meniscus of molten solder which forms on the side of a coupon immersed edge-on into liquid solder bath (Fig. 2). From the height (H) and weight (W) of the risen meniscus, the value of the contact angle was calculated from the following expression:

$$\theta_c = \arcsin \{[4W^2 - (\rho\, g\, P\, H^2)^2] / [4W^2 + (\rho\, g\, P\, H^2)^2]\} \quad (1)$$

where ρ is the solder density, g is the acceleration due to gravity, and P is the sample perimeter. The solder-flux interfacial tension, γ_{LF}, can also be independently determined from the experimental data by the following equation:

$$\gamma_{LF} = (\rho\, g / 4) \{[4W^2 / (\rho\, g\, P\, H^2)] + H^2\} \quad (2)$$

The experimental values of W and H were described by the mean and $\pm$ one standard deviation of five tests per each of these parameters. Maximum and minimum values of H and W were determined by adding or subtracting the standard deviation values from the respective means. These new values were then passed through equations (1) and (2) to compute the maximum and minimum values of θ_c (and γ_{LF}) that served to define their respective scatter values.

The sample coupons were fabricated from oxygen-free high conductivity (OFHC) copper sheet; the coupon dimensions were 1.0 x 1.0 x 0.010 in. Each specimen was solvent degreased; etched in a 1:1 solution (by volume) of HCl and water for 30 s; followed by a rinse sequence and drying. The coupon was then coated with a rosin-based, mildly activated (RMA) flux that was diluted 1:1 (by volume) with isopropyl alcohol and tested per either the wetting balance or meniscometer procedures.

Tests with all solder alloys were performed at a working temperature of 245°C.

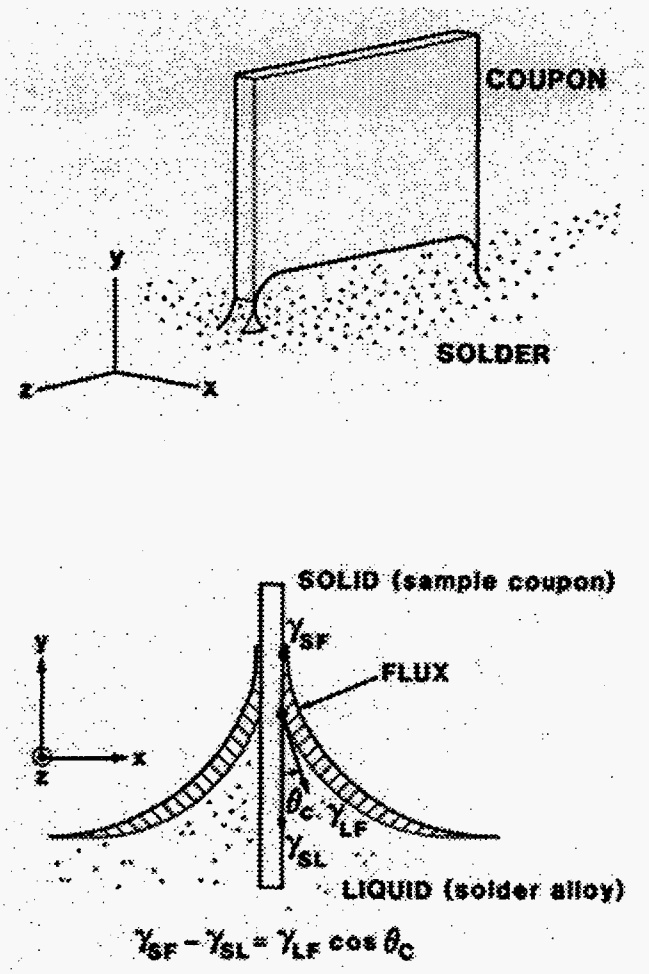

Fig. 2 Schematic diagram of the testing configuration for the wettability evaluation.

2.1.4. Ring-in-plug solder joint shear tests.
The ring-in-plug test methodology was developed as a means to determine the relative *shear* strength of the solder joints. Dimensions of the individual ring and plug piece parts are shown in Fig. 3. OFHC copper was used for the ring and plug structures. The inner diameter of the ring and the outer diameter of the plug results in a nominal solder joint gap of 0.0075 in. The sample preparation/assembly process is summarized as follows: The ring and plug of each specimen was solvent degreased, etched in a solution of HCl and water (see previous section), rinsed and dried. Each piece part was then coated with RMA flux (1:1 solution with isopropyl alcohol). The plug was inserted in the ring with three copper wires, each having a nominal diameter of 0.007 in. The wires maintained concentricity between the ring and the cylinder. An annular preform of the solder alloy was placed about the

juncture between the ring and plug. The entire assembly was placed upon a hot plate set to a temperature of 300°C. The sample remained on the hot plate for a period of 20 s past the point at which the solder preform initially melted. Lastly, the specimen was removed from the hot plate and cooled in an ice bath, and cleaned of flux residues.

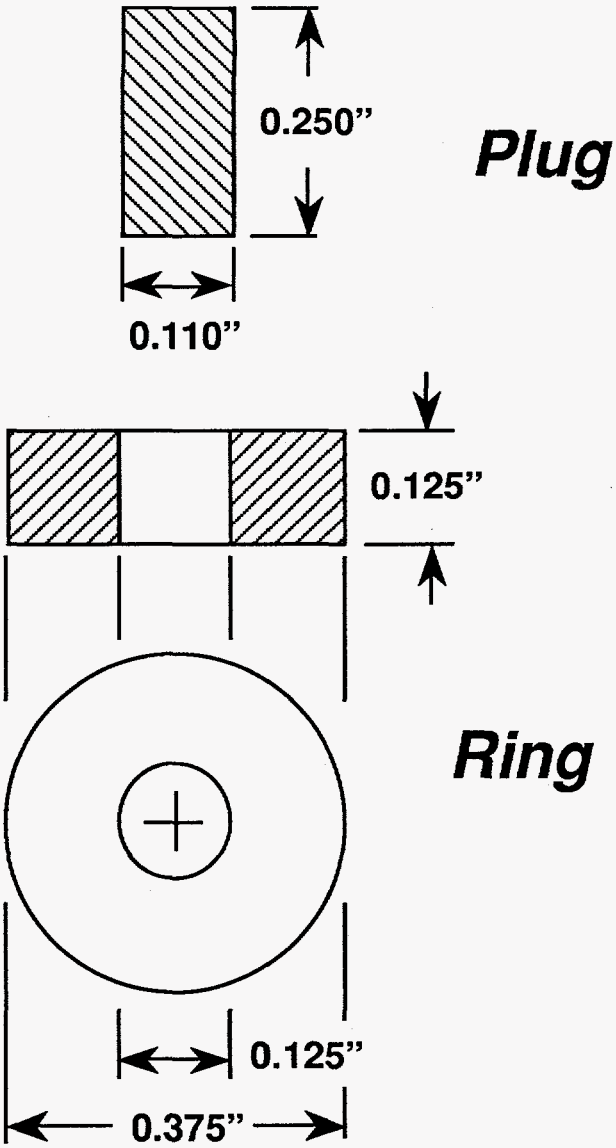

Fig. 3 Ring-in-plug test specimen geometry.

Mechanical testing of the sample comprised pushing the plug through the ring. The extra length of plug that extended beyond the ring was cut off; then, the two broad faces were hand polished to remove any burrs or excess material. The specimens were secured into a specially designed fixture. The fixture was introduced into a loading frame. A ram, which was attached to the cross head member of the load frame, was located directly over the plug. At a crosshead speed of 0.41 in./min, the ram pushed the plug through the ring. The maximum recorded load was used to designate the strength of the joint. Four tests were run per sample category; a fifth specimen was cross sectioned in order to provide a visual inspection of the un-tested solder microstructure. The strength data were represented as the mean and ± one standard deviation of the four measurements.

2.2. Circuit board prototype.

2.2.1. Test vehicle description.

The devices used to evaluate the integrity of the circuit board solder joints were 20 I/O Small Outline Integrated Circuit (SOIC) packages. The package material was plastic. The leads were copper, having the gull wing configuration. The lead pitch was 0.050 in. The lead finishes were either electroplated 63Sn-37Pb solder (which provided the Pb contamination) or hot dipped 100Sn coatings.

The 20 I/O SOIC packages were assembled onto a double-sided, epoxy-glass multifunctional laminate circuit boards with a nominal 0.062 in. thickness. The glass transition temperature of the laminate was between 150°C and 200°C. The copper features were coated with an imidazole-based, organic solderability preservative (3-10 nm). Ancillary data were obtained from additional test vehicles having a hot-air solder leveled (HASL) coating which heightened the Pb contamination levels.

The solders were printed onto the circuit boards as a paste comprised of 89-91 wt.% type 3 metal powder and an RMA flux vehicle. Solder reflow of the test vehicles was performed in an infrared/natural convection furnace under flowing nitrogen (<100 ppm O_2). The nominal furnace parameters were determined in a previous study[11]. The circuit boards were visually inspected after assembly for general defects as well as those that would directly impact the reliability data. Defects of either category were not observed for both solders.

Thermal cycling of selected test vehicles was performed in air. The cycle parameters were: (1) limits, 0°C and 100°C; (2) 5 min holds at the limit temperatures; and (3) 20°C/min ramp rates in either direction. CASTIN™ solder containing specimens were exposed to 0, 2602, 5068, or 10,106 cycles. Solder joints fabricated with the Sn-Ag-Bi alloy were evaluated in the as-fabricated condition (i.e., zero cycles) and after 10,106 thermal cycles.

The microstructure of the SOIC solder joints and their failure morphology were documented by cross section/metallographic techniques and scanning electron microscopy (SEM), respectively.

The mechanical integrity of the gull wing joints was assessed by a pull test procedure. First, the plastic package was cut from the leads. Then, each lead was secured into a small grip fixture that was attached to the cross head of a mechanical test frame. The lead was pulled from the circuit board in a direction perpendicular to the surface. The pull direction, coupled with the gull wing geometry, constituted a *peel-type* mechanical test on the solder joint. The cross head speed of the test frame was 0.35 in./min. Twenty (20) leads were pulled per test; the data were represented as the mean and ± one standard deviation of those multiple data.

3. Results and Discussion.

3.1. Bulk alloy properties measurements.

3.1.1. Thermal properties.

The thermal (melting) properties of the Sn-Pb contaminated solder alloys were documented by DSC. Both the heating and cooling curves were examined. However, emphasis will be placed on the *heating* thermograms. The thermograms of the non-contaminated CASTIN™ and Sn-Ag-Bi solders are shown in Fig. 4. Each alloy exhibited a single (or "primary") peak. The broadening of the Sn-Ag-Bi peak results from the

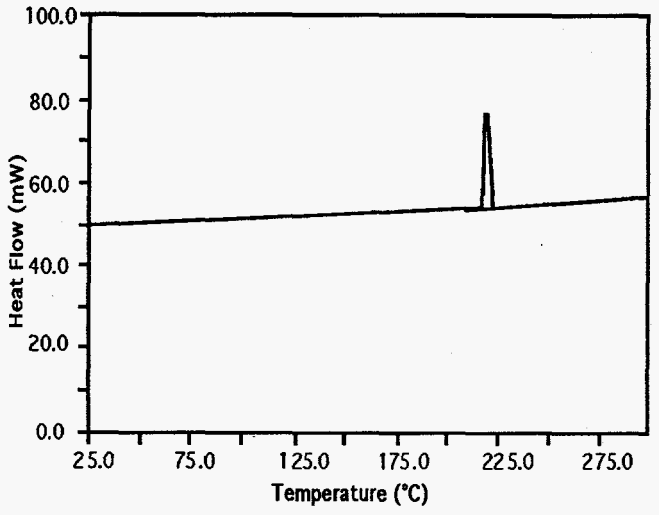

(a)

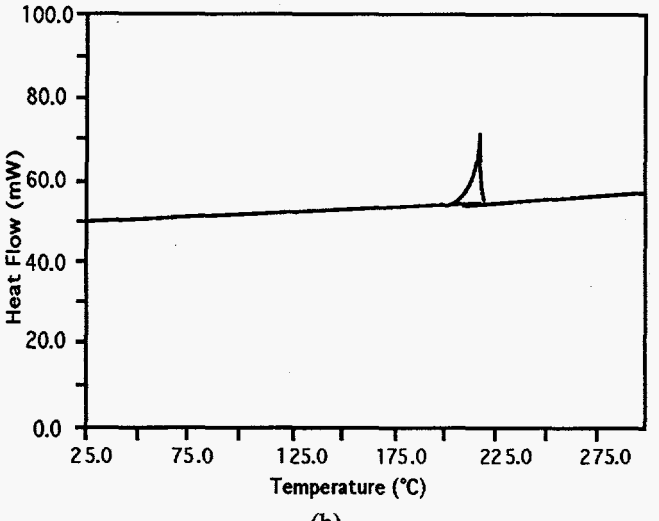

(b)

Fig. 4 DSC thermograms of the non-contaminated (a) CASTIN™ and (b) Sn-Ag-Bi solders. Heating rate: 10°C/min.

so-called "contamination" effect caused by the addition of Bi to the microstructure. As noted earlier, previous studies could not discern separate solidus and liquidus reactions in the Sn-Ag-Bi alloy. The addition of Sn-Pb solder caused the onset temperatures of both solders to *decrease* in the heating and cooling curves. The onset temperatures are plotted as a function of Sn-Pb contamination in Fig. 5 for both solders. The decrease in onset temperature upon heating was greater than that of the cooling curve. Between the two solders, the onset temperature upon heating for the CASTIN™ alloy was more sensitive to the contamination levels than was the Sn-Ag-Bi solder. However; the reverse trend was observed for

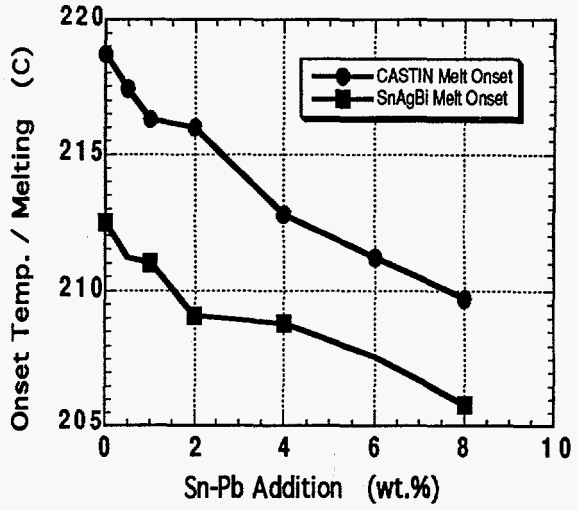

Fig. 5 DSC primary peak onset temperature versus Sn-Pb contamination level for the CASTIN™ and Sn-Ag-Bi solders.

the cooling thermograms. Although the main peaks of both solders broadened towards lower temperatures, the CASTIN™ peak also developed a slight shoulder on the high temperature side starting at 2% contamination. This artifact is typically associated with the development of a melting range, that is, separate solidus and liquidus points.

An important aspect of Sn-Pb contamination for these solders is the generation of additional phases in the microstructure. Of particular concern is the formation of lower melting temperature phases. For example, the eutectic 56Bi-44Pb (wt.%) composition, which has a combined solidus/liquidus temperature of 125°C, can potentially form in the Sn-Ag-Bi solder[12]. As exemplified here, these extraneous phases melt at temperatures well below that of the primary DSC peak. In bulk, as a small fraction of the overall alloy, these phases would not constitute a significant threat to solder integrity by prematurely melting. However, a preference that these phases may have for residing at grain boundary structures in the bulk material, even in small concentrations, can significantly affect the fracture properties (and therefore, overall mechanical integrity) of the solder. This takes place because at the grain boundary, these phases can provide a preferred (or easy) path through which fracture readily occurs.

The DSC thermograms of the two solders were examined for additional, low temperature peaks. No such peaks were detected in the Sn-Ag-Bi data. However, a second peak was found in the DSC results of the CASTIN™ solder, initially at the 2% contamination level. The amplitude of that low temperature peak enlarged with further increases of Sn-Pb levels. The thermogram of the sample with 8% Sn-Pb is shown in Fig. 6. The onset of the low temperature peak is at

approximately 180°C, suggesting that it represents the formation of 63Sn-37Pb colonies within the matrix. Because of the negligible solubility of Pb in Sn, it predicted that the Sn-Pb regions were located along the Sn matrix grain boundaries. In fact, observations of metallographic cross sections confirmed this hypothesis. Fortunately, the Sn-Pb colonies were dispersed throughout the matrix and did not appear to wet the grain boundaries. Therefore, their presence should not significantly affect the mechanical properties (discussed below).

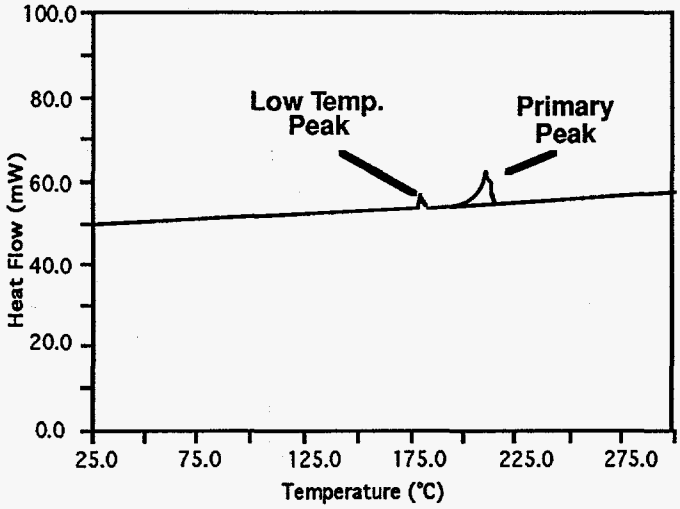

Fig. 6 DSC thermogram of the CASTIN™ alloy contaminated with 8% Sn-Pb. Heating rate: 10°C/min.

3.1.2. Wettability properties.

The contact angle values of the Sn-Pb contaminated CASTIN™ and Sn-Ag-Bi solders are illustrated in Fig. 7. The contact angle of the non-contaminated CASTIN™ solder was 44±6°. As a comparison, the value of θ_c for the traditional 63Sn-37Pb solder (260°C) on Cu, using the same RMA flux, was 17±4°, indicating a more limited wettability of the lead-free CASTIN™ alloy. The contact angles did not change significantly from the baseline level with increased amounts of Sn-Pb contamination. The solder-flux interfacial tension, γ_{LF}, was also observed to be insensitive to Sn-Pb levels, indicating that Sn-Pb contamination did not strongly impact any of the extrinsic or intrinsic wetting properties (θ_c and γ_{LF}, respectively) of the CASTIN™ alloy.

The wettability performance of the Sn-Ag-Bi solder differed from that of the CASTIN™ material. The baseline contact angle of Sn-Ag-Bi solder was 24±6° which is considerably lower than that of CASTIN™ solder, yet greater than that of the 63Sn-37Pb alloy. The contact angle values of Sn-Ag-Bi solder increased significantly with Sn-Pb contamination of 1% and 8% (43±4° and 37±8°, respectively). On the other hand, there was no significant change in θc at Sn-Pb levels of 2% and 4%. These behaviors were further analyzed and observed to reflect changes in the solder-flux interfacial tension, γ_{LF}. That is, the higher values of θc at 1% and 8% were due toincreases in γ_{LF} (450±30 dyne/cm and 440±50 dyne/cm, respectively) above the baseline value (370±30 dyne/cm).

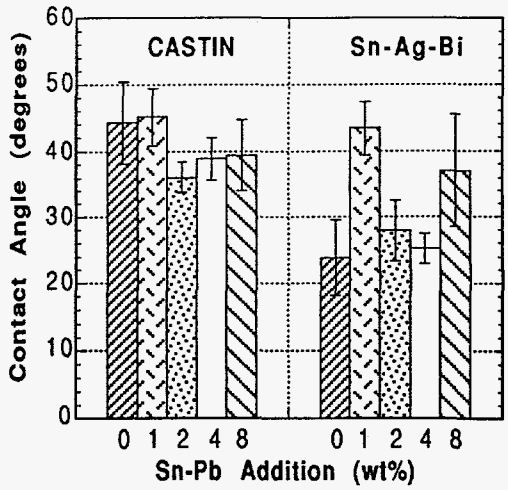

Fig. 7 Contact angle as a function of Sn-Pb contamination for the CASTIN™ and Sn-Ag-Bi solders.

The source of the non-monotonic wetting behavior of Sn-Ag-Bi solder as a function of Sn-Pb contamination level may be caused by an "interaction" between the Bi component of the alloy and the Pb contaminant. By comparing wettability performance of the Sn-Ag-Bi solder with that of the closely related 96.5Sn-3.5Ag solder (43±4°) under similar testing conditions and materials, it is apparent that the Bi addition in the ternary composition is responsible for its lower contact angles. Therefore, interactions between Bi and Pb may curtail the former elements capacity to lower θ_c. However, such interactions are strongly sensitive to the amount of Pb present in the microstructure, and moreover, not with a monotonic dependence upon Pb levels.

3.1.3. Shear strength properties.

The effect which Sn-Pb contamination had on the ring-in-plug shear strength of CASTIN™ and Sn-Ag-Bi solders is summarized in Fig. 8. (For comparison, similarly tested 63Sn-37Pb solder joints exhibit a strength of 270±10 lb). The

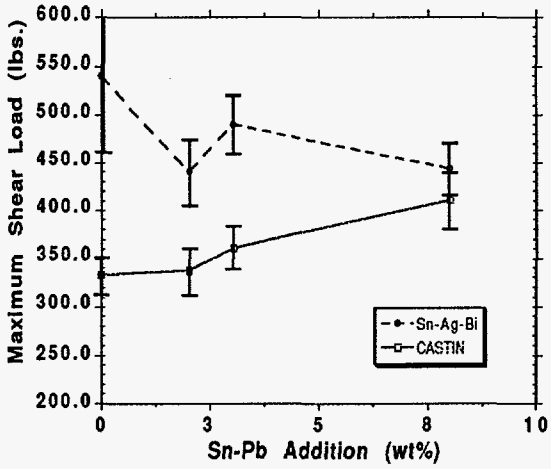

Fig. 8 Maximum ring-in-plug load versus Sn-Pb contamination for the CASTIN™ and Sn-Ag-Bi solders.

CASTIN™ solder exhibited a slight increase in strength with Sn-Pb contamination; however, the increase was significant only at the maximum 8% level. Metallographic cross sections were made of the tested samples in order to determine whether the Sn-Pb contamination had an effect on the failure mode. It was noted that as the Sn-Pb levels increased, the fracture path tended to move closer to the solder/Cu interface, away from the interior of the solder inside of the gap. This point is illustrated by the micrographs in Fig. 9. Shown in Fig. 9a is a

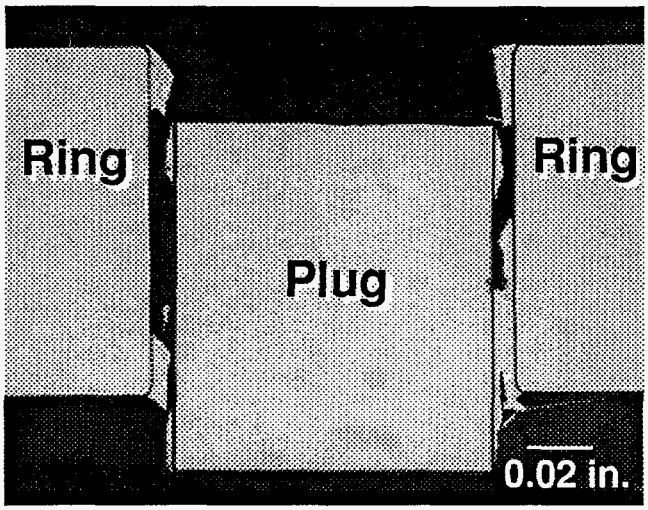

(a)

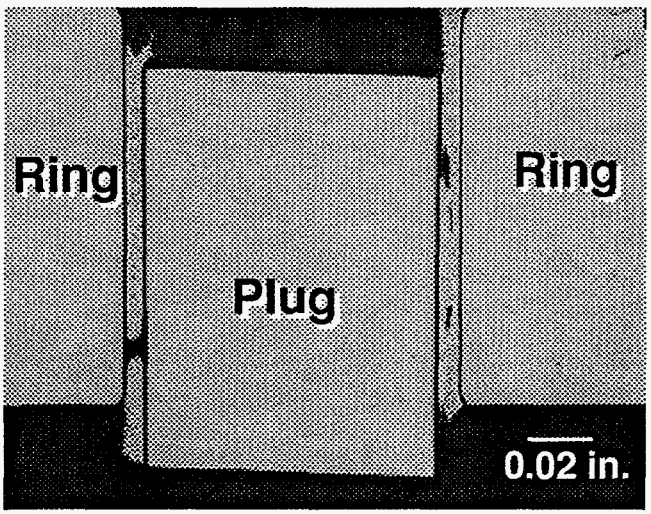

(b)

Fig. 9 Optical micrographs of cross sections of CASTIN™ ring-in-plug specimens after testing: (a) 2% Sn-Pb and (b) 8% Sn-Pb.

cross sectional view of a tested specimen with 2% contamination. A large portion of the failure path was within the solder contained in the gap. When the Sn-Pb contamination level was increased to 8% (Fig. 9b), the fracture path was entirely at the solder/Cu interface. The trends observed in Fig. 9 were corroborated by the strength data in the following summary: As the strength of the CASTIN™ solder increased (with greater Sn-Pb contamination), the failure path moved from of the "bulk" solder and towards the next weakest segment of the joint - the interface. Lastly, the presence of 63Sn-37Pb precipitate regions in the microstructure, as identified by the low temperature peak in the DSC thermograms, was not apparently detrimental to the mechanical strength of the solder (joint).

The strength of the Sn-Ag-Bi ring-in-plug joints showed a substantial decrease with increased Sn-Pb content, particularly at the 8% level. In fact, the strengths of the CASTIN™ and Sn-Ag-Bi solders were similar at the 8% contamination level, in spite of nearly a 200 lb strength difference between the non-contaminated solders. The decrease in strength of the Sn-Ag-Bi solder was not monotonic (as was similarly observed with the wettability data). Observations of the tested specimens revealed no significant dependence by the failure mode on Sn-Pb levels. The joints of the non-contaminated Sn-Ag-Bi solder failed along the solder/Cu interface. (The test sample cross sections appeared similar to that shown in Fig. 9b).

Further study was made to determine more precisely, a source of the strength loss by the Sn-Ag-Bi solder with Sn-Pb contamination. Close examination of photomicrographs of the contaminated Sn-Ag-Bi solder microstructure revealed that Pb was dispersed as particulates throughout the Sn-rich matrix; that is, there was no preferential wetting of the Sn-phase grain boundaries by Pb or the 56Bi-44Pb binary material as was similarly observed with the CASTIN™ solder. However, it appeared that the isolated, elemental Bi precipitates that were observed in the as-fabricated Sn-Ag-Bi solder, had diminished. Inferring a similar fate for the greater amount of Bi contained in solid solution within the Sn-rich phase, it was surmised that Pb did indeed react with the Bi, taking the latter element out of solution from the Sn-rich matrix, and forming the dispersed Pb-Bi particles. Since the Bi content of the ternary Sn-Ag-Bi solder was the principle source of the very high strength of this solder, it being scavenged from the Sn-matrix, to form larger, "inert" precipitates (of Pb) decreased the overall alloy's strength, approaching that of the simple binary 96.5Sn-3.5Ag eutectic composition (370±20 lb). This same mechanism would also explain the loss of wettability suggested in a broader sense, above.

3.2. SOIC solder joint performance.

The as-fabricated solder joints (Fig. 10) exhibited minimal manufacturing defects. This observation corroborated the results of previous manufacturing trials with the CASTIN™ and Sn-Ag-Bi solders[11]. Generally, better wetting was observed for the Sn-Pb coated surfaces as opposed to the imidazole and 100Sn coatings in the case of the CASTIN™ solder; however, the differences were not significantly great so as to affect the solder joint mechanical properties in the as-fabricated condition, or cause premature degradation during thermal cycling.

Metallographic cross sections were made of four solder joints per each of the solder/printed circuit board (PCB) finish/lead finish systems. The microstructure of the as-fabricated joints confirmed good wetting of the leads and circuit board copper features. Plastic deformation, in the form of grain boundary displacement or cracks, was not observed in the solder microstructure of the fillet regions nor in the gap between the

underside of the lead and the circuit board. All indications were that the Sn-Pb surface finishes had readily dissolved into the solder during the assembly process.

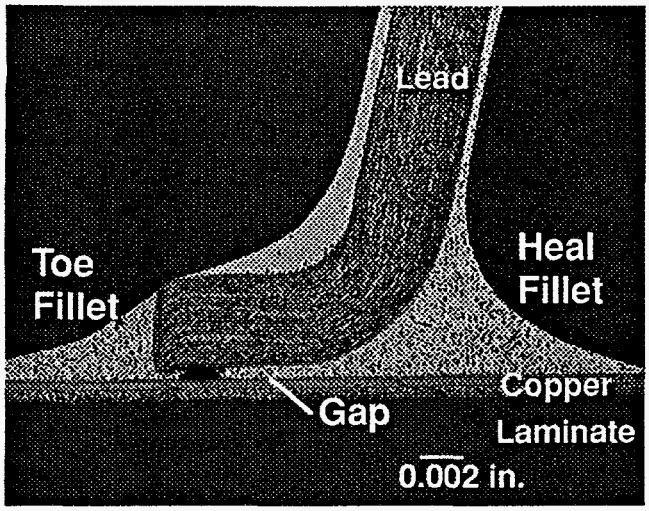

Fig. 10 Optical micrograph of the SOIC gull wing solder joint exemplifying the as-fabricated condition.

Similar metallographic cross sections were made of the corresponding specimens subjected to the nominal 10,000 thermal cycles. Some plastic deformation was observed in the solder microstructure, but it was restricted to the fillet regions of the joint (either the heel fillet or the smaller toe fillet at the end of the gull wing lead). The extent of such damage was limited to surface shear bands and the formation of small cracks in the fillet, typically at the base of the fillet base near the circuit board. Shown in Fig. 11 are optical micrographs which illustrate these features. Fig. 11a illustrates cracking within the heal fillet of a CASTIN™ solder joint formed of Sn-Pb-coated lead and copper pad (HASL). Surface deformation of the toe fillet region is shown in Fig. 11b. No such damage was recorded in the solder microstructure of the more heavily stressed gap region between the lead and the copper pad of the circuit board. The magnitude of the observed deformation was not considered consequential to the integrity (mechanical or electrical) of the solder joints. This point was later supported by the mechanical test results

An initial, quantitative assessment of fillet deformation in the thermally cycled units was performed in order to determine whether the extent of damage was strongly dependent upon lead finish or solder alloy. Each solder joint was separated into a "toe fillet" and a "heel fillet". If damage was observed in that region, the fillet was given a 1 (one); if damage was absent, it was given a 0 (zero). The results from both fillets were combined amongst the four solder joints under observation for the particular solder, PCB finish, and lead finish combination. The quantitative metric was the percentage of "fillets" in each category with damage. The results are shown in Table 1. The data from either solder suggested that the magnitude of the thermal cycle induced deformation was slightly greater with the presence of Sn-Pb from the lead or circuit board finishes.

An additional artifact that was observed solely in the Sn-Ag-Bi/imidazole/Sn-Pb samples was the presence of minor voids and some cracking at the solder/lead interface (Fig. 12). This behavior was rare, being noted in only one (1) of the four (4) joints that were scrutinized.

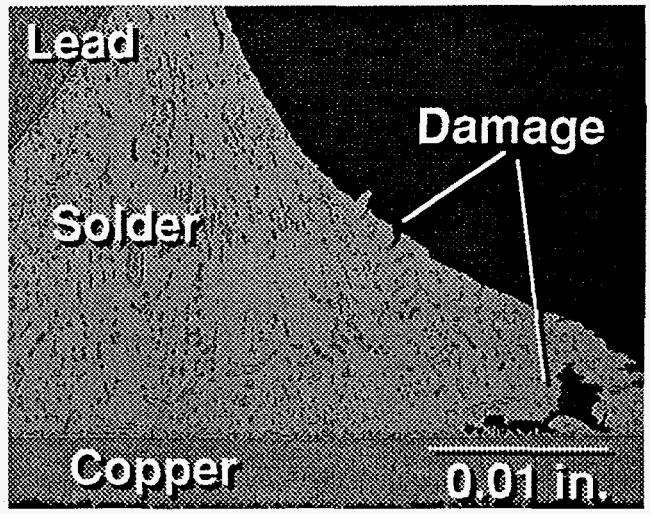

(a)

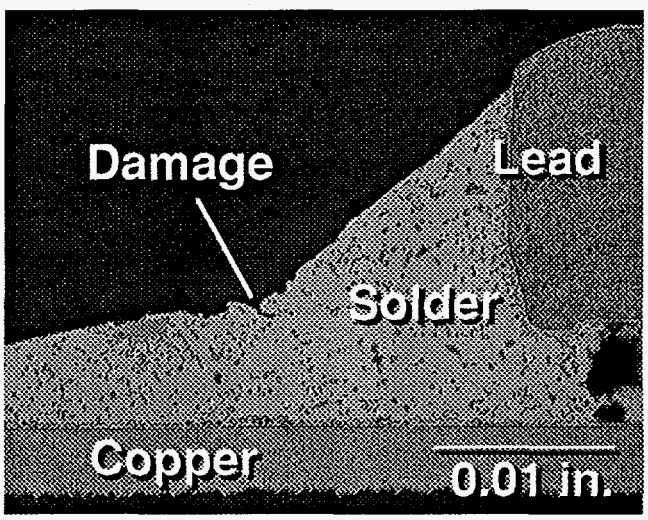

(b)

Fig. 11 Optical micrographs exemplifying fillet damage resulting from 10,106 thermal cycle testing CASTIN™ solder joints assembled from Sn-Pb coated leads and circuit board (HASL): (a) heel fillet crack and (b) toe fillet surface deformation .

The pull strength data for the SOIC leads is presented in Table 2. The strength of as-fabricated joints made with CASTIN™ solder was not sensitive to the circuit board or lead finishes. The strengths were statistically the same, whether the circuit board and lead finishes were: (1) both Sn-Pb (5.42±0.32 lb), (2) imidazole and Sn-Pb, respectively (5.47±0.53 lb); or imidazole and pure Sn, respectively (5.81±0.59 lb).

Thermal Cycles	CASTIN™			Sn-Ag-Bi		
	HASL/Sn-Pb (%)	Imid./Sn-Pb (%)	Imid./Sn (%)	HASL/Sn-Pb (%)	Imid./Sn-Pb (%)	Imid./Sn (%)
0	0	0	0	*****	0	0
10,106	100	63	50	*****	75	50

Table 1 Quantitative assessment of thermal cycle-induced damage to the solder of the solder/PCB finish/lead finish systems.

Thermal Cycles	CASTIN™			Sn-Ag-Bi		
	HASL/Sn-Pb (lb)	Imid./Sn-Pb (lb)	Imid./Sn (lb)	HASL/Sn-Pb (lb)	Imid./Sn-Pb (lb)	Imid./Sn (lb)
0	5.42 +/-0.32	5.47 +/-0.53	5.81 +/-0.59	*****	2.75 +/-0.61	5.31 +/-0.67
2602	4.79 +/-0.97	5.57 +/-0.52	4.22 +/-0.55	*****	*****	*****
5068	4.77 +/-0.82	4.71 +/-0.38	4.05 +/-0.99	*****	*****	*****
10,106	4.24 +/-0.43	4.91 +/-0.68	4.56 +/-0.67	*****	3.13 +/-1.24	5.34 +/-0.74

Table 2 Pull test strength data of the SOIC gull wing leads.

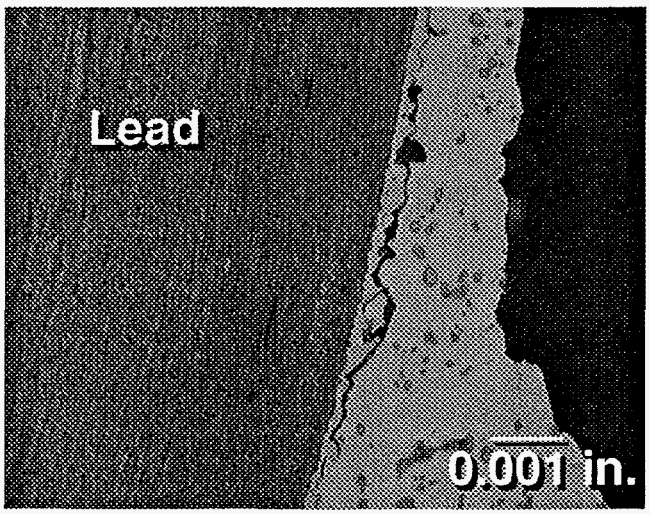

Fig. 12 Optical micrograph of void formation and some minor cracking at the solder/lead interface of the thermally cycled (10,106 cycles), Sn-Ag-Bi/imidazole/Sn-Pb sample.

The fracture morphologies of the CASTIN™ solder joints were sensitive to the coating composition. Shown in Fig. 13 is a scanning electron micrograph of the failure morphology of the circuit board pad from an as-fabricated test vehicle having the imidazole coating; the lead had a Sn-Pb coating. The contour of the failure path followed that of the lead. A similar morphology was observed when the lead finish was changed to pure Sn. However, the fracture path of the joints made with Sn-Pb on both the lead *and* the circuit board pad progressed along the solder/copper pad interface (Fig. 14). This result suggests that the HASL coating caused failure to preferentially occur there. Irrespective of the difference in failure mode, the pull strength of the CASTIN™/HASL/Sn-Pb joints was not significantly different from that of the other joint materials combinations.

The as-fabricated Sn-Ag-Bi/imidazole/Sn solder joints exhibited a pull strength of 5.31±0.67 lb. This value is very similar to that of the CASTIN™ alloy. Recall from the ring-and-plug data that the shear strength of the Sn-Ag-Bi solder was nearly twice that of the CASTIN™ alloy. The source of this apparent discrepancy rests with the different testing modes. As alluded to earlier, the solder/substrate interfaces

each represents a significant material discontinuity in the joint structure. The preference for failure to occur there is dependent upon both the intrinsic strength of the bonding there and the localized stress state. That stress state, and ultimately the "apparent" strength of the joint, will be determined by the mechanical properties of the materials comprising the joint, and the test configuration.

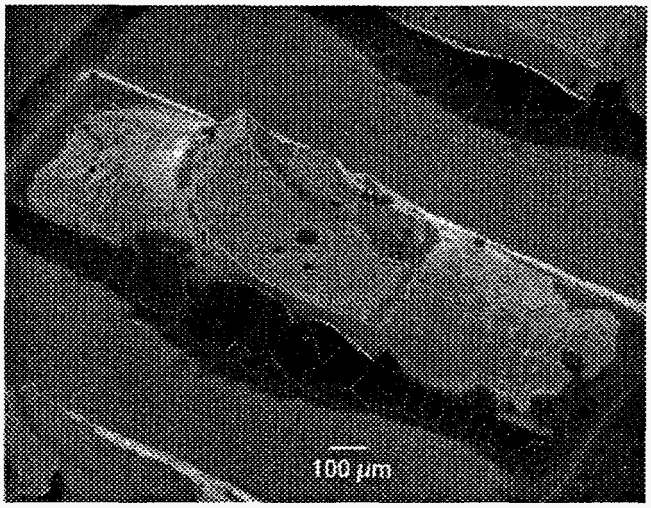

Fig. 13 Scanning electron micrograph of the solder joint pull test failure morphology (circuit board pad) for CASTIN™ solder, imidazole PCB finish, and Sn-Pb lead finish on as-fabricated test vehicles.

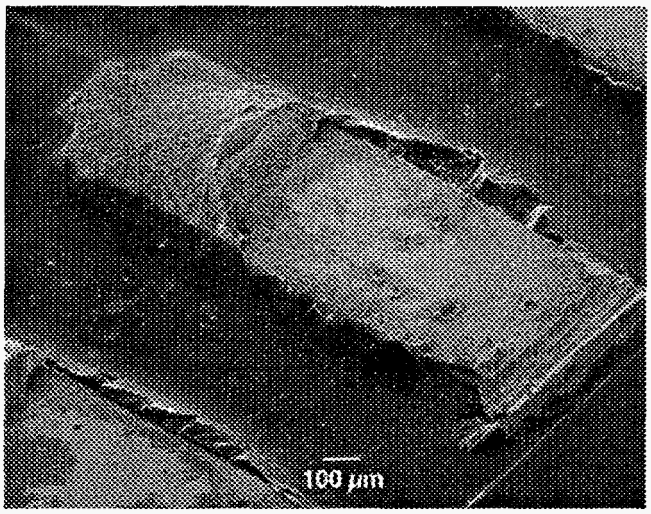

Fig. 14 Scanning electron micrograph of the solder joint pull test failure morphology (circuit board pad) on as-fabricated test vehicles with CASTIN™ solder, Sn-Pb (HASL) PCB finish, and Sn-Pb lead finish .

Test configuration is an important variable, when all else is equal (i.e., materials and joint processing), because it can determine the stress state in the joint (bulk solder and interfaces) and therefore, where failure occurs. For example, the interface strength will appear greater when tested under shear, such as in the ring-in-plug test format, than when tested with a tensile component, such as in the SOIC lead pull test. Therefore, in the former case, the joint strengths will more closely represent the bulk solder properties. In this latter case, failure is more likely to occur at the interface, reflecting the generally weaker strength of the interface under tension. Since the interfaces of the CASTIN™ and Sn-Ag-Bi solders have similar microstructure, their strengths would be similar. This hypothesis was substantiated by the data in Table 2.

Referring to Table 2, it was observed that the use of a Sn-Pb lead finish with the Sn-Ag-Bi solder caused a precipitous drop in the joint pull strength, to a value of 2.75±0.61 lb. If it is assumed that the intrinsic strength of the interface was unaffected by the Sn-Pb coating, then this behavior suggests a significant decline in the strength of bulk solder strength, reaching values that were comparable to, or lower than that of the interface.

The ring-in-plug tests showed that Sn-Ag-Bi solder exhibited a decrease in bulk strength with increasing Sn-Pb content. However, although the ring-in-plug data appear to corroborate the loss in Sn-Ag-Bi solder joint strength with Sn-Pb contamination, it is beneficial to further substantiate this concept by determining whether the bulk Sn-Ag-Bi solder strength *could* have been sensitive to the Sn-Pb contamination levels arising from the lead. Therefore, the Sn-Pb concentration levels in the SOIC gull wing joints were estimated. Two calculations were performed. The first analysis assumed that the Pb content had completely diffused throughout the joint. In the second computation, it was assumed that the Pb contaminants remained localized. For the latter condition, the gap between the lead and the circuit board was selected (at a thickness of 0.002 in.) because the limited Sn-Ag-Bi solder volume there would provide a "worst case" contamination level.

Estimates of the Sn-Pb concentration in the joints were based on typical joint geometries observed in the metallographic cross sections. It was also assumed that the Sn-Pb coating layer of the lead had a thickness of 0.0003 in. The results of the computations showed that in the first case of complete interdiffusion, the expected Sn-Pb contamination would be approximately 10 wt.%. In the second scenario of localized Sn-Pb contamination build-up, the Sn-Pb concentration in the joint gap was calculated to be about 18 wt.%. An extrapolation of the ring-in-plug data in Fig. 8 indicates that the bulk Sn-Ag-Bi solder will experience a significant strength loss from the gull wing Sn-Pb coatings. Therefore, the effect of Sn-Pb contamination on the bulk Sn-Ag-Bi solder strength is a viable cause of the loss of pull strength in the contaminated SOIC solder joints.

The morphology of the fracture surfaces for all of the as-fabricated Sn-Ag-Bi solders were similar to those observed in Fig. 13.

The impact which thermal cycling had on the pull strength of the CASTIN™ solder joints was dependent upon the particular circuit board/lead finish (Table 2). In the case of a Sn-Pb finish on both the circuit board (HASL) and on the leads, the post-thermal cycle pull strengths were lower than the baseline (zero cycles) value of 5.42±0.32 lb; however, the decrease became significant only after 10,106 thermal cycles

(4.24±0.43 lb). The fracture morphology did not differ from that of the as-fabricated pull test specimens. The microstructural damage observable in the thermally cycled parts, did not appear to have a strong role in the failure modes of the solder joints. Therefore, the source of lower strengths for the thermally cycled joints were smaller scale changes to the microstructure of the solder that remained unobservable.

The pull strength of the CASTIN™/imidazole/Sn-Pb joints decreased slightly with thermal cycling; however, the lower strengths were not significantly different from the baseline value following any of the exposure conditions. The fracture morphology likewise remained unchanged from that of the as-fabricated units.

The CASTIN™/imidazole/Sn solder joints, on the other hand, exhibited strength drops that were significant in all cases of thermal cycling. From a baseline value of 5.81±0.59 lb, the pull strength decreased to 4.22±0.55 lb, 4.05±0.99 lb, and 4.56±0.67 lb after 2602, 5068, and 10,106 thermal cycles, respectively. When these data were compared with those from the other two test categories, the values were similar. That is, a large extent of the apparent strength loss was due to a relatively high as-fabricated (initial) strength (again, relative to the other data).

It was noted from metallographic cross sections that the drop in strength accompanying the Sn-Pb additions was not caused by large-scale damage in the solder microstructure (i.e., cracks); such damage can potentially jeopardize the *electrical* performance of the joint. Also, thermal cycling did not alter the fracture morphology of the solder joints. Finally, the strength levels of the Sn-Pb contaminated CASTIN™ solder joints were more than adequate to provide mechanical integrity for the package.

The test results from the CASTIN™ solder joints indicated that there was no significant trend to pull strength versus Sn-Pb contamination level after thermal cycling. That is, Sn-Pb contamination did not consistently accelerate, nor retard, the extent of pull strength loss in the SOIC solder joints caused by thermal cycling. Based upon the earlier estimates of the Sn-Pb contamination levels to be expected in the gull wing joints (which would be further increased in the PCB HASL finish specimens), and the fact that at those levels, 63Sn-37Pb compositional phases would certainly form in the solder (from earlier DSC data), then the presence of those regions did not deteriorate the as-fabricated pull strength, nor did they cause an adverse effect on joint strength and integrity under the thermal aging conditions which accompanied the thermal cycling tests. Therefore, it may be inferred that the 63Sn-37Pb regions, which form in CASTIN™ solder by excess (<2%) Sn-Pb contamination, are relatively stable under *general* elevated temperature environments, and are not likely to pose a threat to joint reliability under extended service conditions.

Finally, the pull strengths of thermally cycled joints made with the Sn-Ag-Bi solder were examined (Table 2) In this case, only the 10,106 thermal cycled specimens were evaluated. It was observed that the strengths were unchanged from the respective values of the as-fabricated samples (zero thermal cycles). The lower strength of the joints made from leads with the Sn-Pb solder, relative to the strength of joints having leads with pure Sn finishes, remained the case after thermal cycling. The consistent solder joint pull strengths were accompanied by no apparent changes to the fracture surface morphology, as well. The magnitude of the Sn-Ag-Bi solder joint strengths would clearly support the attachment function in all cases. Since the decreases in strength caused by Sn-Pb contamination were not accompanied by cracks or other discontinuities in the solder, electrical integrity would not be jeopardized. Therefore, although the pull strength of the Sn-Ag-Bi solder was sensitive to the extent of Sn-Pb contamination, those strength levels were not further impacted by exposure to the thermal cycling environment, suggesting similar long term reliability as was predicted for the CASTIN™ solder.

Conclusions

1. The wettability, melting properties, and ring-in-plug shear strength of two lead-free solders were examined as a function of 63Sn-37Pb contamination over the range of 0<wt.%<10. The study was extended to examine the performance of 20 I/O SOIC solder joints on prototype test vehicles.

2. Both the 96.2Sn-2.5Ag-0.8Cu-0.5Sb (CASTIN™) and 91.84Sn-3.33Ag-4.83Bi (Sn-Ag-Bi) solders exhibited decreases in melting onset temperatures with increased Sn-Pb contamination, the effect being greater in the former case. The CASTIN™ solder also developed a secondary, low temperature peak at 183°C for Sn-Pb levels en excess of 2%, indicating the formation of 63Sn-37Pb zones. Also, the CASTIN™ solder developed a high temperature shoulder to the main peak, suggesting the start of separation by the eutectic peak into separate liquidus and solidus events.

3. The wettability of CASTIN™ solder on Cu with an RMA flux was not statistically sensitive to Sn-Pb contamination. Although the baseline wetting performance of the Sn-Ag-Bi solder was better than that of the CASTIN™ alloy, a significant increase was observed at 1% and 8% Sn-Pb. At the other Sn-Pb levels, there was no effect.

4. The Cu ring-in-plug shear strength of CASTIN™ joints increased slightly with Sn-Pb contamination, being significantly greater only at 8%. On the other hand, the Sn-Ag-Bi solder exhibited a decrease in shear strength with similar contamination levels.

5. The pull strength of as-fabricated, SOIC gull wing joints assembled with CASTIN™ solder were not sensitive to the presence of Sn-Pb from the lead and/or circuit board Sn-Pb coatings. Although the strength drop observed after thermal cycling was sensitive to the presence of Sn-Pb in the finish, the post-thermal cycle strengths (and microstructural integrity) were adequate to meet attachment requirements.

6. In the case of the Sn-Ag-Bi solder, nearly 50% lower pull strengths were measured with Sn-Pb contamination from the package lead coatings. However, the strength levels remained unchanged following 10,106 thermal cycles. Since the lower strength values were satisfactory for package attachment and damage to the microstructure appeared to be inconsequential,

the Sn-Ag-Bi solder remained a viable alternative solder for Sn-Pb coated substrates.

Acknowledgments

The authors wish to thank Cindy Hernandez for her assistance with the wetting tests; Alice Kilgo and Charlie Carter for metallographic sample preparation and optical micrographs; and Barry Ritchie for his scanning electron microscopy efforts. This work was supported in part by the U.S. Dept. of Energy through work performed at Sandia National Laboratories under contract DE-AC04-94AL85000.

References

[1] The Montreal Protocols, 1987.

[2] Artaki, I, et al., "Fine Pitch Surface Mount Technology Assembly with Lead-free, Low Residue Solder Paste," *Soldering and Surface Mount Tech.*, May 1995, p.27.

[3] Artaki, I., et al., "Wave Soldering with Pb-Free Solder", *Proc. Surface Mount Inter.*, (SMTA, Edina, MN; 1995), p.495

[4] Vianco, P. and Mizik, P., "Prototyping Lead-Free Solders on Hand-Soldered, Through-Hole Circuit Boards," *Proc. 7th SAMPE Conf.*, ed. B. Rasmussen, et al., (SAMPE, Corvina, CA; 1994), p.366.

[5] Vianco, P. and May, C., "An Evaluation of Prototype Surface Mount Circuit Boards Assembled with Three Non-Lead Bearing Solders," *Proc. Surface Mount Inter.*, (SMTA, Edina, MN: 1995), p.481.

[6] Vianco, P., et al., "Development of a Sn-Ag-Bi Solder for Electronic Applications," TMS Fall Meeting, Rosemont, IL., (1994).

[7] McCormick, M. and Jin, S., "Progress n the Design of New Lead-Free Solder Alloys," *J. of Metals* 45 (1993), p.36.

[8] Lee, N-C, et al., "A Novel Lead-Free Solder Replacement,", *Proc. Surface Mount Inter.*, (SMTA, Edina, MN; 1994), p.463.

[9] Vianco, P. and Rejent, J., "Tin-Silver-Bismuth Solders for Electronics Applications," U.S. Patent 5,439,639 (1995).

[10] Vianco, P., "An Overview of the Meniscometer/Wetting Balance Technique for Wettability Measurements," *The Metal Science of Joining*, ed. M. Cieslak, et al, (TMS, Warrendale, PA; 1992), p.265.

[11] Jackson, A., et al., "Manufacturing Feasibility of Several Lead-Free Solders for Electronic Assembly," *Proc. 7th SAMPE Conf.*, (SAMPE, Corvina, CA; 1994), p.381.

[12] *Binary Alloy Phase Diagrams*, ed. T. Massalski, et al., (TMS, Warrendale, PA; 1986), p.524.

DISCLAIMER